15TH IEA HEAT PUMP CONFERENCE
MAY 26–29, 2026 | HOFBURG
VIENNA 2026
DECARBONISATION THROUGH INNOVATION

Numerical study of GAX ammonia-water absorption chiller using plate heat exchangers

PHAM Van Kha [a,b,c], LE PIERRÈS Nolwenn [a], PHAN Hai Trieu [b,*]

[a] Laboratoire procédés énergie bâtiment (LOCIE) – CNRS, Université Savoie Mont Blanc, Savoie Technolac, 73370 Le Bourget du Lac, France
[b] Université Grenoble Alpes, CEA, LITEN, DTCH, L2TS, F-38000 Grenoble, France
[c] University of Transport and Communications, No 3. Cau Giay Street, Hanoi, Vietnam

Abstract

A generator/absorber heat exchange (GAX) absorption cooler using waste heat or solar energy with the ammonia-water (NH_3-H_2O) working pair to produce cooling down to -20 °C is a potential solution to reduce electricity consumption and greenhouse gas emissions. Previous parametric studies of the GAX cycle were mostly conducted under the assumption of constant heat exchanger effectiveness. In this study, a new model was developed based on effectiveness values determined for different operating conditions to improve the accuracy of the simulation. The results showed a significant reduction in deviation between simulation results and experimental data when the thermal and mass effectiveness parameters were optimally adjusted. Specifically, the average relative deviation of the cooling capacity and the coefficient of performance (*COP)* decreased from 16 % to 1.6% and from 8% to 2%, respectively. Furthermore, the developed model was applied to evaluate the impact of the two-phase state of the refrigerant at the inlet of the condenser, which can reduce the machine performance by up to 10%.

Keywords: Absorption chiller; GAX architecture; Plate heat exchanger; Modeling; NH_3-H_2O

1. Introduction

Absorption chillers using renewable heat sources are expected to partially replace vapour compression chillers to reduce the need for electricity and greenhouse gas emissions in the future [1]. This transition would be eased with an improved efficiency of the machine along with a more compact size [2]. This can be achieved by using a generator-absorber heat exchange (GAX) NH_3-H_2O absorption cycle. In this cycle, part of the heat rejected during the absorption process is recovered to generate the refrigerant vapor (as will be detailed in Figure 1). This reduces the external heat required at the generator [3,4].

Several studies on the simulation of the GAX refrigeration cycle have been carried out. Grossman et al. [5] studied a GAX absorption cycle with a cooling capacity of 10 kW, the evaporation temperature of 10 °C, a condenser/ absorber temperature of 42 °C, and a generator temperature of 195 °C. The heat transfer characteristics of some heat exchangers are included in the model through *UA* values. Absorption simulation (ABSIM) software was used to solve and the simulated Coefficient Of Performance (*COP*) is about 1.04. Simulation results were also obtained for off-design conditions. However, this model has not been validated experimentally.

* Corresponding author: haitrieu.phan@cea.fr

Also, Herold and Keith [6] simulated a GAX NH_3-H_2O absorption chiller with a cooling capacity of 468 kW. With generator temperature, absorber temperature and evaporator temperature conditions of 163, 40 and 5 °C, respectively, the *COP* achieved was 1.11. This study was conducted with the assumption of ideal heat exchange for the GAX, the rectifier and the generator so it is difficult to achieve the above efficiency with actual machines.

In the work by Mendiburu et al. [7], the authors built a more detailed simulation model for the GAX cycle. The model has divided the important heat exchanger components in the system (such as the generator and rectification column and GAX heat exchanger) into many control volumes and formulated balance equations for each of those elements. The absolute relative errors for the *COP* compared with the experimental study of Gomez et al. [8] (heating oil temperature entering the generator was 193 °C, cold water temperature produced was 15.3 °C) and the simulation of Herold and Keith [6] were 1.47 % and 1.07 %, respectively. The comparison results are good under design conditions with the assumption of a 5 °C approach temperature for the GAX heat exchangers. However, evaluations under other conditions have not yet been carried out.

The above simulation results have shown that the GAX cycle can achieve a *COP* greater than 1 under cooling conditions with positive temperatures. Other conditions with negative temperatures, however, have not yet been investigated. To further expand the application of absorption chillers, the FriendSHIP project developed an innovative design using the GAX effect with a commercial plate heat exchanger (PHE) to produce chilled water down to -20 °C using renewable energy sources as well as improving compactness and facilitating industrialization. Aste and Phan [9] conducted a numerical study of the above cycle and obtained a *COP* of 0.45 at an ambient temperature of 20 °C and a generator temperature of 120 °C. Later, Demasles et al. [10] built a prototype with a cooling capacity of 10 kW. A numerical model was also developed to compare with the prototype. The results showed a deviation of about 5% for the *COP* and 20% for the cooling capacity.

The literature review indicates that most numerical parametric studies have been conducted under the assumption that the parameters in the heat exchanger models (e.g., approach temperature, *UA*, or effectiveness) are constant. However, the actual efficiency parameter in plate heat exchangers vary with operating conditions [11,12]. Moreover, in the GAX cycle, the performances of the heat recovery components strongly influence the overall efficiency [6,10,13,14]. Therefore, the objective of this study is to develop a thermodynamic model of the GAX cycle that enhances accuracy by considering the variation of heat exchangers parameters with respect to operating conditions. Simulations are carried out to determine the optimal effectiveness values under the specified experimental conditions. The validated model is then applied to detailed analyses, such as assessing the influence of a two-phase state at the condenser inlet.

2. Cycle description and experimental results

The architecture of the GAX prototype was developed in the FriendSHIP project [10] and shown in Figure 1. It consists of the main heat exchangers of the conventional absorption cycle (a generator, absorber, evaporator, condenser, rectifier, pre-cooler) and additional heat exchangers: GAX-1 and GAX-2. This architecture allows taking advantage of the GAX effect, where heat can be received from the absorption process (GAX-1) as well as heat recovery from the weak solution (GAX-2) and the rectifier to preheat and desorb the solution. To improve compactness, all the above components are selected as plate heat exchangers. Tanks ST21, ST22, and ST3 are used to separate heat transfer, mass transfer, and phase separation, thereby improving the functioning of the heat exchangers. The working principle of the prototype can be divided into three sub-cycles as follows:

2.1. Strong solution sub-cycle

From state 11, the strong solution is pumped to a higher pressure at state 12. It then passes through GAX-1, the rectifier, and GAX-2 to recover heat before entering the generator at state 21. At GAX-1, the solution is preheated from the first absorption process and reaches state 13. After that, the solution splits into two branches: one branch (13,P) exchanges heat with the rectifier to become state 14,A, while the other branch (13,b) passes through the bypass valve (which is used to regulate the rectifier temperature). These two flows are mixed into state 14, which is further heated by the weak solution (from 22 to 23) and becomes state 15. Then, it enters separator tank ST21, separating to vapor (310) and solution (21). The solution flows to the generator, where external heat raises it to state 211. It then enters separator ST22 and split into vapor (311) and weak solution (22).

2.2. Refrigerant sub-cycle

The vapors from states 310 and 311 combine and pass through the rectifier. After purification, it goes to ST3, where the flow is separated into vapor that has been purified (state 32) and condensate (state 41). The purified vapor at state 32 flows to the condenser and becomes liquid at state 33. It is subcooled in the pre-cooler to state 34, then expanded through the valve to state 35. At the evaporator, the refrigerant evaporates and absorbs heat from the chilled fluid, producing cooling down to -20 °C. The refrigerant leaves the evaporator as low-pressure vapor at state 36. It is then reheated in the pre-cooler to state 37.

2.3. Weak solution sub-cycle

The weak solution at state 23 mixes with the condensate at state 41, forming state 24. This state, after throttling at the solution valve, becomes a low-pressure weak solution (state 25). In GAX-1, the first absorption process occurs between the weak solution at state 25 and the vapour at state 37, releasing heat that preheats the strong solution from state 12 to state 13 as stated before. The remaining solution at the outlet of the GAX-1 (state 26) is fully absorbed into the strong solution at state 11 through an exothermic process, and the released heat is transferred to an external fluid.

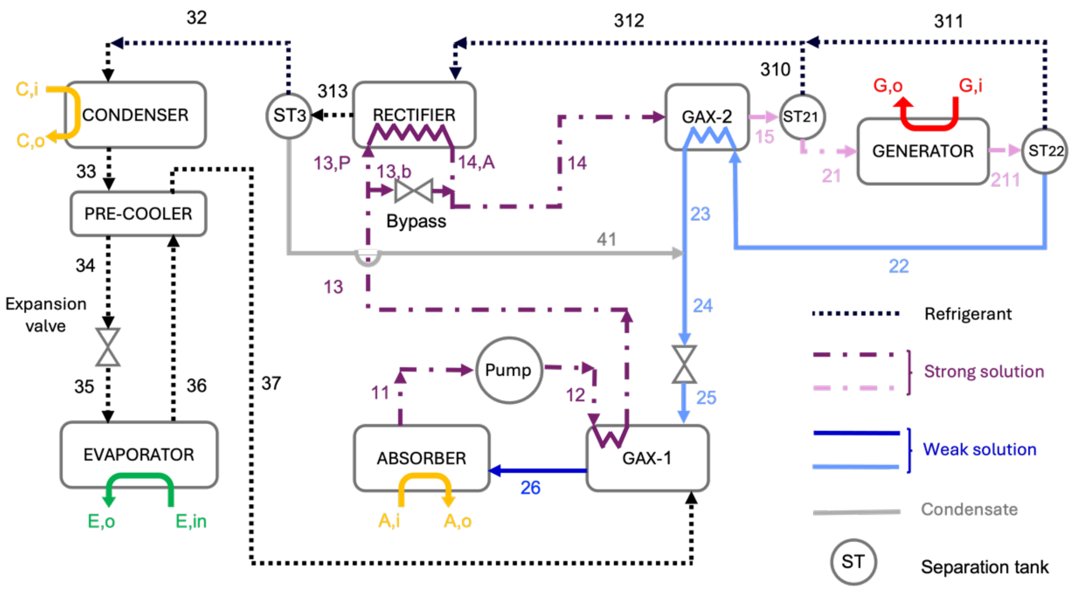

Figure 1. Schematic diagram of the GAX-absorption chiller.

The type and uncertainty of the instrumentation are introduced in detail in the study of Demasles et al. [10]. The uncertainty of temperature is 0.1 K and the uncertainty of the refrigerant mass flow rate is given in the Table 1.

The heat flux of the absorber, the generator, the condenser and the evaporator are calculated from the heat transfer fluid (HTF) mass flow rate follows as:

$$\dot{Q} = \dot{m}_{HTF} \times Cp_{HTF} \times (T^{*,out} - T^{*,in}) \tag{1}$$

The *COP* of this prototype is defined as the ratio between the useful energy at the evaporator and the heat input in the generator:

$$COP = \frac{\dot{Q}_E}{\dot{Q}_G} \tag{2}$$

Table 1 presents the operating conditions of the GAX prototype and the experimental results of the cooling capacity and the *COP* with the uncertainties determined by the propagation of uncertainties method [15].

During the data analysis, the state of the vapor leaving the separator and entering the condenser (state 32) is always in a two-phase condition. Therefore, to evaluate its influence the vapor quality is considered. The vapour quality (q) is defined as the ratio of the mass of vapour over the total mass. In this study, q_{32} is determined from T_{32}, P_{32} and x_{32} assuming $x_{32} = x_{34}$ and $p_{32} = p_{33}$, where x_{34} is determined from the measured values $T_{34}, p_{33}, \rho_{34}$ according to a correlation obtained using EES software [16].

Table 1. Experimental data of stabilized points at different heat transfer fluid temperatures with calculations of uncertainty for pump mass flow rate, vapour quality at the condenser inlet, the evaporator power and the *COP*.

Test	$T_G^{*,in}$ [°C]	$T_A^{*,in}$ [°C]	$T_C^{*,in}$ [°C]	$T_E^{*,out}$ [°C]	$\dot{m}_{pump}$ [kg/h]	q_{32} [kg/kg]	$\dot{Q}_E$ [kW]	COP [-]
#1	120.1	19.6	19.8	-19.2	171.7 ± 0.08	0.960 ± 0.013	5.88 ± 0.51	0.38 ± 0.03
#2	120.2	19.8	19.9	-15.2	172.4 ± 0.09	0.976 ± 0.013	5.95 ± 0.71	0.39 ± 0.05
#3	130.1	19.7	19.9	-19.5	171.6 ± 0.08	0.962 ± 0.013	6.33 ± 0.43	0.37 ± 0.03
#4	130.1	19.4	19.7	-9.7	171.0 ± 0.12	0.979 ± 0.011	9.01 ± 0.43	0.46 ± 0.02
#5	130.1	19.7	20.0	-7.4	169.5 ± 0.14	0.983 ± 0.011	9.92 ± 0.42	0.49 ± 0.02
#6	140.1	19.7	19.9	-19.4	169.8 ± 0.09	0.965 ± 0.013	6.29 ± 0.41	0.36 ± 0.03

3. Numerical study

In this study, a model of the GAX absorption chiller was built, using the measured data presented previously. For the internal heat exchangers, this model employed thermal and mass effectivenesses which were either constant or determined by adjusting the simulation results to match the experimental data.

3.1. Hypothesis

To simulate the operation of the GAX refrigeration cycle, a zero-dimensional model was developed. The following general assumptions are used [6,13,17–20]:

- The system is at steady state;
- The evaporator, condenser, generator and separation tanks are considered equilibrium;
- Components and pipes are adiabatic;
- Pressure drops are negligible;
- Expansion through the valves is considered isenthalpic;
- The mixing point is adiabatic;
- Pump work could be neglected.

3.2. Thermodynamic models

The general mass, species and energy conservation equations are applied for each component and mixing point (Eq. (3) – Eq. (5)):

$$\sum \dot{m}_{in} - \sum \dot{m}_{out} = 0 \tag{3}$$

$$\sum \dot{m}_{in}\, x_{in} - \sum \dot{m}_{out}\, x_{out} = 0 \tag{4}$$

$$\sum \dot{m}_{in}\, \mathrm{h}_{in} - \sum \dot{m}_{out}\, \mathrm{h}_{out} + \sum \dot{Q} + \sum \dot{W} = 0 \tag{5}$$

Heat exchanger (HE)

In this study, to reduce the complexity improve the numerical convergence and focus on the analysis of the heat exchangers that exhibit the GAX phenomenon, a pinch point model is used for the generator, the absorber, the condenser and the evaporator [6]. The outlet temperature of the generator, absorber, condenser and evaporator is determined by the heat transfer fluid (HTF) temperature and the minimum temperature difference ΔT^{min} (Eq. (8) - Eq. (12) in Table 2). ΔT^{min} values were set based on the values assessed experimentally (Table 3). The evaporator temperature glide ΔT_E^{glide} is maintained in the prototype at 3 °C by the refrigerant throttling valve.

Thermal effectiveness models were used for the pre-cooler, GAX-1, GAX-2 and rectifier (Eq. (13) – Eq. (19)). Thermal effectiveness is defined as the ratio between the actual power transferred to the maximum transferable power [21].

$$\varepsilon_{th} = \frac{\dot{Q}}{\dot{Q}_{max}} \tag{6}$$

According to our experimental results, the thermal effectiveness of the pre-cooler reached 0.99 and was used in all simulation cases.

The efficiency of the absorption process is affected by both heat and mass transfer [22]. Therefore, in the simulation study of the GAX cycle, the mass effectiveness model is used, specifically for GAX-1 and the absorber (Eq. (20) - Eq. (23)). The mass effectiveness is the ratio of the concentration differences between the inlet and the outlet to the concentration differences between the inlet and an ideal saturated outlet [10]:

$$\varepsilon_{mass} = \frac{x_{in} - x_{out}}{x_{in} - x_{out,sat}} \tag{7}$$

Most of the models determine that the thermal and mass effectiveness are constant under all working conditions [6,10,13,14]. However, the efficiency of heat and mass transfer is sensitive to the operating conditions, which in turn affects the cycle efficiency [6,23,24]. Therefore, in this study, the thermal and mass effectiveness is selected according to each operating conditions to improve the accuracy of the model.

Separation tank

The separation process is assumed to occur at constant pressure and temperature. Normally, the exiting vapour and liquid of the separation tanks are considered to be saturated [10]. However, the experimental results of the prototype show that the outlet of ST3 to the condenser is two-phase. The experimental average vapour quality is 0.971 (Table 1). Details of the evaluation and analysis of this is presented in the results and discussion section 4.

Bypass

Demasles et al. [10] studied the effect of the rectification temperature on the refrigerant concentration and hence on the COP of the cycle. The results showed that maintaining the rectification temperature at 75 °C can give the highest efficiency. Therefore, a bypass valve was installed to maintain this temperature at point 313. The coefficient bypass is expressed through the bypass factor MR_{bypass} (Eq. (24), Eq. (25)). The value of the bypass factor was determined under the different operating conditions (Table 3).

Expansion valve

In some studies, the pressure of the cycle is determined based on the assumption that the liquid leaving the evaporator and condenser is saturated [14,25]. However, according to the analysis of the prototype, the saturations at outlet of the evaporator and condenser do not occur [26]. Therefore, to improve the accuracy of the simulation model, the low pressure is determined by Eq. (28) and the high pressure is determined by the refrigerant expansion valve model (Eq. (29) – Eq. (30)). The relationship between the refrigerant flow rate and the *Kv* coefficient is determined by fitting the experimental values (Eq. (30)).

The equations describing the GAX cycle model are solved using the EES software [16] according to the flow chart shown in Figure 2.

Table 2. Summary of specific components equations model of the GAX cycle.

Components	Equations	
Evaporator, Generator, Condenser, Absorber	$T_{35} = T_E^{*,out} - \Delta T_E^{min}$	(8)
	$T_{36} = T_{35} + \Delta T_E^{glide}$	(9)
	$T_{211} = T_G^{*,in} - \Delta T_G^{min}$	(10)
	$T_{33} = T_C^{*,in} + \Delta T_C^{min}$	(11)
	$T_{11} = T_A^{*,in} + \Delta T_A^{min}$	(12)
GAX-1, GAX-2, Rectifier, Pre-cooler	$T_{hot,out,id} = T_{cold,in}$	(13)
	$h_{hot,out,id} = h(T_{hot,out,id}, P_{hot}, x_{hot})$	(14)
	$T_{cold,out,id} = T_{hot,in}$	(15)
	$h_{cold,out,id} = h(T_{cold,out,id}, P_{cold}, x_{cold})$	(16)
	$\dot{Q}_{PHE,max} = \min\,[\dot{m}_{cold} \times (h_{cold,out,id} - h_{cold,in});\ \dot{m}_{hot} \times (h_{hot,in} - h_{hot,out,id})]$	(17)
	$\varepsilon_{th} = \frac{\dot{Q}_{PHE}}{\dot{Q}_{PHE,max}}$	(18)
	$\dot{Q}_{PHE} = \dot{m}_c \times (h_{c,out} - h_{c,in}) = \dot{m}_h \times (h_{h,in} - h_{h,out})$	(19)
GAX-1	$x_{26,liq,sat} = x(T_{26}, P_{26}, q_{26} = 0)$	(20)
	$\varepsilon_{mass,GAX-1} = \frac{x_{26,liq} - x_{25}}{x_{26,liq,sat} - x_{25}}$	(21)
Absorber	$x_{11,liq,sat} = x(T_{11}, P_{11}, q_{11} = 0)$	(22)
	$\varepsilon_{mass,A} = \frac{x_{11} - x_{26,liq}}{x_{11,liq,sat} - x_{26,liq}}$	(23)

Bypass	$\dot{m}_{13,P}=\dot{m}_{13} \times MR_{bypass}$	(24)
	$\dot{m}_{13,b}=\dot{m}_{13} \times (1- MR_{bypass})$	(25)
Expansion valves	$h_{25} = h_{24}$	(26)
	$h_{35} = h_{34}$	(27)
	$P_{low} = P(T_{35}, x_{35}, h_{35})$	(28)
	$\dot{m}_{34} = Kv \times \sqrt{P_{high} - P_{low}}$	(29)
	$Kv = 0.3964 \times \dot{m}_{34} - 0.00031$	(30)

Comparison between experimental and modeling results was evaluated by using the absolute relative error (*ARE*) and the average of the absolute relative error (*AARE*) [7]:

$$ARE\ (\%) = \frac{|Exp.value - simulation\ value|}{Exp.value} \times 100\% \tag{31}$$

$$AARE\ (\%) = \frac{1}{6} \times \sum_{i=1}^{6} ARE_i \tag{32}$$

The criteria for $ARE_{\dot{Q}_E}(\%)$, $ARE_{\dot{Q}_G}(\%)$, $ARE_{COP}(\%)$ are required to be lower than the uncertainty value. Under the above conditions, some sets of effectiveness parameters can be obtained. The objective of the simulation is to investigate the system behavior, particularly the vapour generation thanks to by the GAX exchanger and the generator. Therefore, an additional criterion of $ARE_{\dot{m}}(\%)$ to be less than 10% is introduced. To find the optimal effectiveness set, the thermal effectiveness values are varied from 0.6 to 1.0, while the mass effectiveness ranges from 0.3 to 0.8. At each iteration, the values are increased sequentially by 0.01.

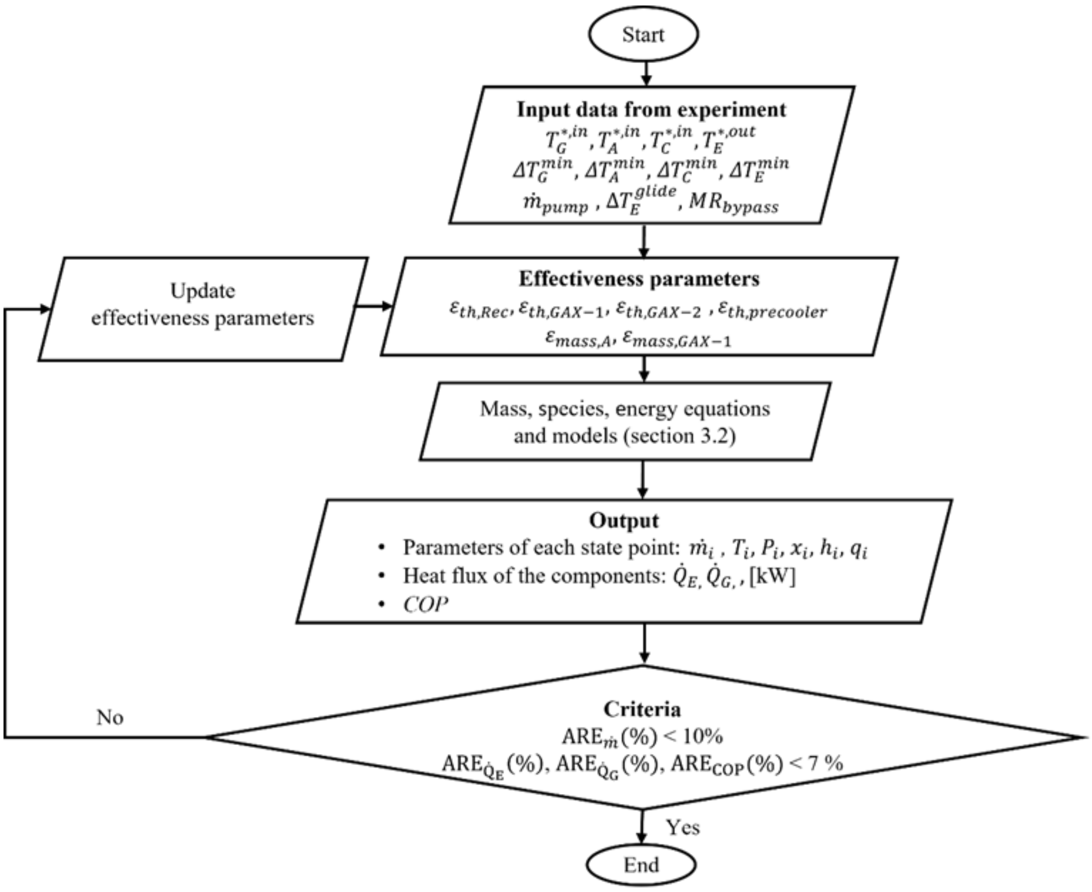

Figure 2. Flowchart for the chiller simulations with iterations to calculate the optimized values of thermal and mass effectiveness to satisfy the predefined criteria concerning the mass flow rate, the evaporator and generator powers and the *COP*.

Table 3. Input values of the bypass ratio and the pinch temperatures at the generator, the absorber, the condenser and the evaporator obtained through experimental tests.

Test	MR_{bypass}	ΔT_A^{min} [°C]	ΔT_C^{min} [°C]	ΔT_E^{min}[°C]	ΔT_G^{min}[°C]
#1	0.174	2.0	0.7	4.3	2.6
#2	0.223	2.0	0.2	4.0	2.6
#3	0.310	2.2	0.0	4.5	2.8
#4	0.300	2.3	2.7	5.1	3.2
#5	0.304	2.8	2.9	5.1	3.0
#6	0.435	2.5	0.0	4.5	2.9

4. Results and discussion

4. 1. Simulations with fixed and optimized thermal and mass effectiveness

The results presented in this sections are simulated with inputs from the Table 1 and Table 3. First, simulations will be performed with fixed effectiveness values for thermal effectiveness of GAX-1, GAX-2 and the rectifier of 0.8, while mass effectiveness of GAX-1 and the absorber is 0.6 [10]. The results of the optimized effectiveness parameters according to the Figure 2 are given in Table 4. In most of the working conditions GAX-2 and the rectifier have thermal effectiveness higher than the fixed value of 0.8. Mass effectiveness in all cases is less than 0.6.

Table 4. The resulted values of the thermal and mass efficiencies of different internal heat exchangers (GAX-1, GAX-2, Rectifier, Absorber) obtained from the calculations by the flowchart in Figure 2.

Test	$\varepsilon_{th,GAX-1}$	$\varepsilon_{th,GAX-2}$	$\varepsilon_{th,REC}$	$\varepsilon_{m,A}$	$\varepsilon_{m,GAX-1}$
#1	0.85	0.66	0.90	0.53	0.49
#2	0.77	0.76	0.70	0.45	0.41
#3	0.85	0.90	0.74	0.47	0.54
#4	0.75	0.90	0.90	0.50	0.60
#5	0.75	0.90	0.92	0.52	0.51
#6	0.85	0.95	0.88	0.44	0.47
Average	**0.80**	**0.85**	**0.84**	**0.49**	**0.50**

Figure 3 presents the comparison between the fixed-value case (with the thermal effectiveness of 0.8 and the mass effectiveness of 0.6) and the case with optimized effectiveness parameters. With the fixed-parameter model, no experiment simultaneously satisfies both $\dot{Q}_E$ and *COP* criteria. In contrast, when the effectiveness parameters are adjusted to vary with the operating conditions, both $\dot{Q}_E$ and *COP* criteria are achieved with errors smaller than the experimental uncertainty. The results further show that the *AARE* of $\dot{Q}_E$ and *COP* decreases from 15.9% to 1.6% and from 8.0% to 2.1%, respectively, when optimizing the effectiveness parameters. One reason for the improvement in model accuracy is that the simulation error of the mass flow rate decreases significantly, from 42.8% in the fixed-parameter case to 4.2% in the optimized case.

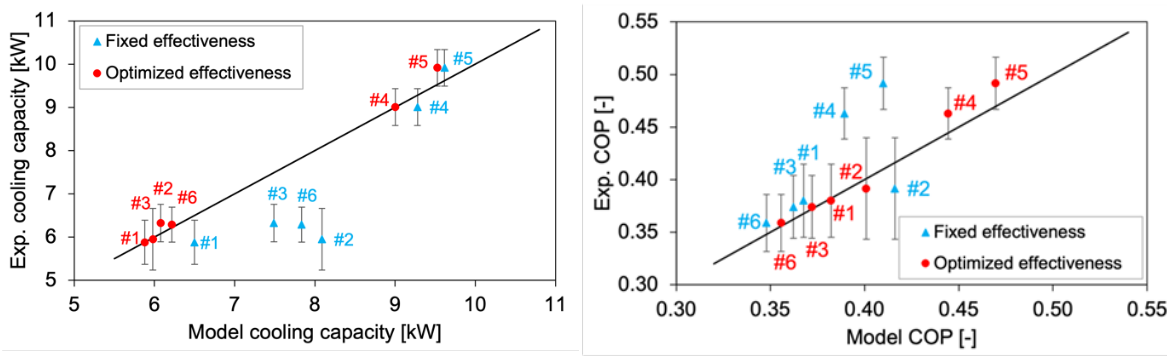

Figure 3. Comparison of the cooling capacity and the *COP* between two methods: simulations with fixed values versus simulations with optimized values of thermal and mass effectiveness, with the reference of experimental data.

4.2. Simulations with saturated vapour and two-phase conditions

To evaluate the influence of refrigerant vapour quality at the condenser inlet, a comparison is made between the commonly assumed saturated vapour condition (*q_32=1)* and the two-phase vapour condition (*q_32=0.971)* using the optimized efficiencies model. The results for $\dot{Q}_E$ and *COP* in both cases are presented in Figure 4. In all simulations, the saturated vapour condition is consistently greater than the two-phase vapour condition for both $\dot{Q}_E$ and *COP*. The calculations indicate that the presence of only a small fraction of liquid in the vapour leads to an average reduction of 9.8 % in $\dot{Q}_E$ and 11.4 % in *COP*. This occurs because, in the model, the concentration of the refrigerant is determined by temperature, pressure, and vapour quality at the condenser inlet. Thus, even a small amount of liquid carried with the vapor into the condenser reduces the refrigerant concentration. Consequently, the evaporation process becomes less effective, the amount of ammonia actually evaporated decreases, and the overall cooling capacity and *COP* are reduced. These findings suggest that improving vapour quality at the condenser inlet could significantly enhance the prototype's performance.

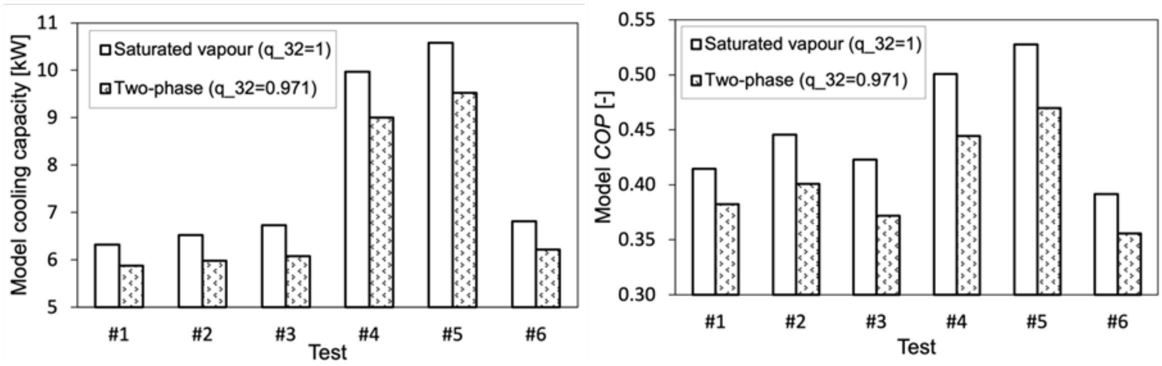

Figure 4. Comparison of the cooling capacity and the *COP* of simulations with saturated vapour (q_32 = 1) versus simulations with vapour containing a small amount of liquid (q_32 = 0.971) at the condenser inlet.

5. Conclusions

By using the pinch temperature model and the optimized thermal and mass effectiveness values obtained from a prototype's experimental data, a new simulation model of an NH_3-H_2O GAX absorption refrigeration cycle was proposed. The simulation results showed that adjusting parameters such as the thermal effectiveness of GAX-1, GAX-2 and the rectifier as well as the mass effectiveness of absorber and GAX-1, under different working conditions, reduces the average deviation between simulation and experimental values of the cooling capacity and the *COP* to about 1.6 % and 2.1% respectively. In addition, the impact of the two-phase flow entering the condenser was observed. The carry-over of liquid solution droplets lowers the overall NH_3 concentration in the refrigerant sub-cycle and subsequently degrades the cooling capacity. Specifically, only about 2.9 % of liquid at the condenser inlet can reduce the cooling capacity and the *COP* of the machine by 9.8 % and 11.4 % respectively.

One limitation of the current model is its dependence on existing experimental data to determine the effectiveness values. To extend its applicability, a model employing correlations for the heat exchanger effectiveness will be developed to predict system behavior under different operating conditions.

Nomenclature

h	specific enthalpy, kJ/kg	out	outlet
$\dot{m}$	mass flow rate, kg/s	***Subscripts***	
MR_{bypass}	bypass factor, -	A	absorber
p	pressure, bar	C	condenser
q	vapour mass quality, kg/kg	E	evaporator
$\dot{Q}$	heat exchange rate, kW	G	generator
T	temperature, °C	HTF	heat transfer fluid
T^*	temperature of heat transfer fluid,	id	ideal
°C		in	inlet

UA	heat transfer conductance, kW/K	liq	liquid
$\dot{W}$	power, kW	max	maximum
x	ammoniac mass fraction, kg/kg	out	outlet
Greek Symbols		R	rectifier
ρ	density, kg/m^3	sat	saturated
ε	heat exchanger effectiveness	th	thermal
Superscripts		***Acronyms***	
in	inlet	*ARE*	absolute relative error
min	minimum	*AARE*	average absolute relative error
COP	coefficient of performance	GAX	generator/absorber heat exchange
EES	engineering equation solver	HTF	heat transfer fluid
Exp.	experimental	PHE	plate heat exchanger

Acknowledgements

Van Kha Pham received funding from the Vietnam Government Scholarship (Project 89, decision n° 2314/QĐ-BGDĐT dated 11/08/2023). The authors would like to express their gratitude to the French Alternative Energies and Atomic Energy Commission for the funding of this research (Contract n° C46726). We would like to thank the members of the European FriendSHIP project (Grant Agreement n° 884213) for their valuable research contributions and providing us with the experimental data used in this study.

References

[1] Hara Chakravarty K, Sadi M, Chakravarty H, Sulaiman Alsagri A, James Howard T, Arabkoohsar A. A review on integration of renewable energy processes in vapor absorption chiller for sustainable cooling. Sustainable Energy Technologies and Assessments 2022;50:101822. https://doi.org/10.1016/j.seta.2021.101822.

[2] Altamirano A, Stutz B, Le Pierrès N. Experimental Characterization of a Three-Dimensional-Printed Adiabatic Desorber for Absorption Chillers. Heat Transfer Engineering 2022;43:1867–84. https://doi.org/10.1080/01457632.2021.2022301.

[3] Jawahar CP, Saravanan R. Generator absorber heat exchange based absorption cycle—A review. Renewable and Sustainable Energy Reviews 2010;14:2372–82. https://doi.org/10.1016/j.rser.2010.05.002.

[4] Pham VK, Pierrès NL, Phan HT. Overview of Research on NH3-H2O Absorption Heat Pump and Refrigeration Cycles Including Generator/Absorber Heat-Exchangers. Heat Transfer Engineering 2025:1–28. https://doi.org/10.1080/01457632.2025.2578965.

[5] Grossman G, DeVault RC, Creswick FA. Simulation and Performance Analysis of an Ammonia-Water Absorption Heat Pump Based on the Generator-Absorber Heat Exchange (GAX) Cycle, Chicago, Illinois, United States: 1995.

[6] Herold KE, Radermacher R, Klein SA. Absorption Chillers and Heat Pumps. 2nd ed. Boca Raton: CRC Press; 2016. https://doi.org/10.1201/b19625.

[7] Mendiburu AZ, Roberts JJ, Rodrigues LJ, Verma SK. Thermodynamic modelling for absorption refrigeration cycles powered by solar energy and a case study for Porto Alegre, Brazil. Energy 2023;266:126457. https://doi.org/10.1016/j.energy.2022.126457.

[8] Gómez VH, Vidal A, Best R, García-Valladares O, Velázquez N. Theoretical and experimental evaluation of an indirect-fired GAX cycle cooling system. Applied Thermal Engineering 2008;28:975–87. https://doi.org/10.1016/j.applthermaleng.2007.06.027.

[9] Aste F, Phan HT. Numerical study on multi-effect and multi-stage NH3/H2O absorption chillers for negative cooling in SHIP systems, 2021, p. 140001. https://doi.org/10.1063/5.0149485.

[10] Demasles H, Muller A, Phan HT. Development of ammonia-water absorption chillers for negative cooling in industrial solar systems, Paris, France: 2023. https://doi.org/10.18462/iir.icr.2023.0054.

[11] Braccio S, Phan HT, Wirtz M, Tauveron N, Le Pierrès N. Simulation of an ammonia-water absorption cycle using exchanger effectiveness. Applied Thermal Engineering 2022;213:118712. https://doi.org/10.1016/j.applthermaleng.2022.118712.

[12] Ko J-W, Bae KJ, Kwon OK. Correlation development on heat and mass transfer of absorber tube for absorption chiller. Applied Thermal Engineering 2025;265:125467. https://doi.org/10.1016/j.applthermaleng.2025.125467.
[13] Dixit M, Arora A, Kaushik SC. Thermodynamic analysis of GAX and hybrid GAX aqua-ammonia vapor absorption refrigeration systems. International Journal of Hydrogen Energy 2015;40:16256–65. https://doi.org/10.1016/j.ijhydene.2015.09.048.
[14] Jawahar CP, Saravanan R, Bruno JC, Coronas A. Simulation studies on gax based Kalina cycle for both power and cooling applications. Applied Thermal Engineering 2013;50:1522–9. https://doi.org/10.1016/j.applthermaleng.2011.11.004.
[15] Wheeler AJ, Ganji AR. Introduction to engineering experimentation. Third edition. Upper Saddle River, N.J.: Pearson Higher Education; 2010.
[16] Klein SA. Engineering Equation Solver (EES) v11.922 2024.
[17] Mohammadi K, Saghafifar M, McGowan JG, Powell K. Thermo-economic analysis of a novel hybrid multigeneration system based on an integrated triple effect refrigeration system for production of power and refrigeration. Journal of Cleaner Production 2019;238:117912. https://doi.org/10.1016/j.jclepro.2019.117912.
[18] Kholghi SA, S. Mahmoudi SM. Energy and exergy analysis of a modified absorption cycle: A comparative study. Sustainable Energy Technologies and Assessments 2019;32:19–28. https://doi.org/10.1016/j.seta.2019.01.002.
[19] Mehr AS, Zare V, Mahmoudi SMS. Standard GAX versus hybrid GAX absorption refrigeration cycle: From the view point of thermoeconomics. Energy Conversion and Management 2013;76:68–82. https://doi.org/10.1016/j.enconman.2013.07.016.
[20] Shi Y, Wang Q, Hong D, Chen G. Thermodynamic analysis of a novel GAX absorption refrigeration cycle. International Journal of Hydrogen Energy 2017;42:4540–7. https://doi.org/10.1016/j.ijhydene.2016.10.155.
[21] Wirtz M. Development of a falling-film desorber combining vapor generation and purification for ammonia-water absorption chiller (Modeling and Experiments). PhD Thesis. Université Savoie Mont Blanc, 2022.
[22] Islam MdR, Wijeysundera NE, Ho JC. Heat and mass transfer effectiveness and correlations for counter-flow absorbers. International Journal of Heat and Mass Transfer 2006;49:4171–82. https://doi.org/10.1016/j.ijheatmasstransfer.2006.04.002.
[23] Kim B. Heat and Mass Transfer in a Falling Film Absorber of Ammonia—Water Absorption Systems. Heat Transfer Engineering 1998;19:53–63. https://doi.org/10.1080/01457639808939926.
[24] Scharfe J, Ziegler F, Radermacher R. Analysis of advantages and limitations of absorber-generator heat exchange. International Journal of Refrigeration 1986;9:326–33. https://doi.org/10.1016/0140-7007(86)90004-6.
[25] Xu ZY, Gao JT, Hu B, Wang RZ. Multi-criterion comparison of compression and absorption heat pumps for ultra-low grade waste heat recovery. Energy 2022;238:121804. https://doi.org/10.1016/j.energy.2021.121804.
[26] Pham VK, Phan HT, Le Pierrès N. Experimental analysis of the refrigerant two-phase flow in an absorption chiller based on GAX cycle, Congress of the Société Français de Thermique, Chambéry, France: 2025. https://doi.org/10.25855/SFT2025-043.